Cell-Autonomous and Systemic Circadian Regulation of Gene Expression in Adipocytes

Jennifer M. Worthen[1, *], Armina-Lyn M. Frederick[1], Phillip A. Dumesic[2], Jennifer J. Loros[1], Jay C. Dunlap[1,3, *]

[1] Department of Molecular and Systems Biology, Geisel School of Medicine at Dartmouth, Hanover, New Hampshire 03755, USA

[2] Diabetes Center, University of California, San Francisco, California 94143, USA

[3] Lead contact

[*] For correspondence: Jennifer M. Worthen (jennifer.marie.worthen@dartmouth.edu); Jay C. Dunlap (jay.c.dunlap@dartmouth.edu)

Running title: Circadian Gene Regulation in Adipocytes

ABSTRACT

Circadian clocks strongly influence adipocyte biology. Studying adipocyte circadian regulation in the absence of organismal cues isolates cell-autonomous clock control, providing insight into mechanisms relevant to metabolic disease. To resolve circadian core biological programs, we deeply sequenced bulk RNA from inguinal-derived, *in vitro*-differentiated adipocytes (IVDAs) over 2.5 days and compared clock-controlled genes (CCGs) with existing mouse supraclavicular brown (BAT) and epididymal white (eWAT) adipose tissue circadian time-course datasets. Using Phase Set Enrichment Analysis (PSEA), we report 21% of the protein-coding transcriptome is rhythmic in IVDAs. Intrinsic circadian regulation governs key processes in energy metabolism, molecular transport and transcription. Integration with *in vivo* datasets reveals that BAT and IVDAs exhibit more cohesive rhythmic pathways than does eWAT, clustering around the late-night early-morning transition. To explore how these pathways may be regulated, we reexamined a recent interscapular BAT cistrome dataset. Using IVDA transcription factors

that were phase-aligned (≤4hr) with *in vivo* as input, motif enrichment analysis revealed two temporally distinct regulatory programs; an early E-box activator ARNT-family/bHLH-PAS program was enriched for transcriptional regulation, RNA metabolism, and signaling pathways, and a late nuclear receptor-associated program enriched for energy metabolism, phospholipid biosynthesis, mitochondrial function, ECM organization, and nuclear receptor signaling. Overall, we identify novel rhythmic transcripts and define cell-autonomous circadian programs in adipocytes whose timing is further sculpted by systemic cues *in vivo*. Because obesity is associated with adipocyte hypertrophy and hyperplasia, processes likely influenced by circadian regulation, these findings advance our understanding of clock-controlled adipocyte metabolism and its contribution to metabolic dysfunction.

INTRODUCTION

The circadian clock plays a central role in regulating metabolism by synchronizing physiological processes to the 24h daily cycle (Bass, 2012; Hurley et al., 2016; Schrader et al., 2024). In nearly every animal cell, this internal timekeeper coordinates key functions such as energy expenditure and intermediary metabolism (van Rosmalen et al., 2024; Neufeld-Cohen et al., 2016; Malik et al., 2024). While studies of adipose tissue *in vivo* have established the rhythmic nature of adipose tissue function, the extent to which these rhythms are cell-intrinsic versus systemically driven remains unclear. Adipocytes integrate nutrient availability, hormonal signals, and energetic demand and retain the capacity for autonomous circadian regulation. Clocks in adipose tissues drive rhythmic expression of genes and proteins critical to nutrient metabolism, signaling, and secretion, which influence glucose homeostasis and energy balance (Zvonic et al., 2006; Rosen and Spiegelman, 2006; Hepler and Bass, 2023). Adipose tissue is composed of several cell types, including mesenchymal stem cells, immune cells and vascular cells, with distinct anatomical depots serving specialized functions (Sakers et al., 2022; Yang Loureiro et al., 2022; Corvera et al., 2026). In addition, recent single-cell and single-nucleus studies have demonstrated substantial heterogeneity among adipocytes within individual depots, revealing multiple transcriptional states and functional subpopulations (Loft et al., 2025). While all white adipose tissue

53 (WAT) stores energy as triglycerides in lipid droplets, brown adipose tissue (BAT) is also dense with
54 mitochondria and constitutively capable of dissipating chemical energy as heat by adaptive non-shivering
55 thermogenesis (ANST) (Bunk et al., 2025; Rahbani et al., 2024; Sun et al., 2021; Cannon and
56 Nedergaard, 2004; Puigserver et al., 1998). Interspersed throughout inguinal WAT (iWAT) and other
57 depots is a subtype transiently capable of ANST, referred to as "brown in white" or beige (Vargas-Castillo
58 et al., 2024; Bertholet et al., 2017; reviewed in Inagaki et al., 2016). Over-feeding or cold exposure via
59 sympathetic nervous system activation induces a metabolic sink via H^+ leakage across the mitochondrial
60 membrane or futile phosphorylation cycling, and this is retained through epigenomic memory (Roh et al.,
61 2018). While the physiological relevance and mechanisms underlying this plasticity are debated (Cypess
62 et al., 2025), the upregulation of an ANST-like response in adipocytes is, in part, driven by cell-
63 autonomous sensing of ambient cold (Ye et al., 2013).
64
65 The circadian oscillator comprises a self-regulating transcriptional-translational feedback loop (TTFL).
66 The core clock proteins CLOCK and BMAL1 form a heterodimer that enters the nucleus and binds to E-
67 box sequences on target clock-controlled genes (CCGs) to initiate transcription (Takahashi, 2017; Van
68 Drunen and Eckel-Mahan, 2021; Rasmussen et al., 2022). Upregulated genes include paralogs of
69 Cryptochrome (*Cry*) and Period (*Per*), whose products form multimeric complexes with casein kinase
70 1d/e; these interact with CLOCK:BMAL1, resulting in their inhibition by blocking the activity of
71 CLOCK and BMAL1 at E-boxes and thereby also reducing *Per/Cry* expression (Smyllie et al., 2025).
72 Serial phosphorylation of the CRY and PER proteins by CK1 eventually relieves inhibition, allowing the
73 cycle to reinitiate *Cry* and *Per* expression (Cao et al., 2021; Narasimamurthy and Virshup, 2021; Philpott
74 et al., 2023; Ricci et al., 2025).
75
76 Disruption of circadian rhythms is strongly associated with metabolic dysfunction, including obesity and
77 insulin resistance. When food or physical activity, very strong temporal cues, are shifted out of the active
78 phase and into the resting phase, body composition as well as other parameters of metabolic health are

79 altered (Acosta-Rodríguez et al., 2022; Acosta-Rodríguez et al., 2024), yet it remains unclear which
80 aspects of adipocyte metabolic regulation arise from intrinsic clock control versus systemic cues
81 including feeding, temperature, and neuroendocrine input (Allada and Bass, 2021; Fekry and Eckel-
82 Mahan, 2022, Schrader et al., 2024). Resolving this distinction is essential for understanding how
83 temporal regulation of adipocyte metabolism contributes to health and disease (Deota et al., 2025).
84 Indeed, circadian regulation in adipose tissue has significant implications. In mice, chronic circadian
85 shifts drive WAT hypertrophy, inflammation, and disrupted metabolic regulation, resulting in obesity-like
86 transcriptional changes and impaired insulin signaling (Xiong et al., 2021). Circadian disruptors like shift
87 work and jet lag alter adipokine expression and secretion, linking disrupted rhythms to metabolic
88 dysfunction (Kettner et al., 2015; Scheer et al., 2009; Kiehn et al., 2017; Samanta and Ali, 2022). Brown
89 adipose-specific deletion of *Arntl/Bmal1* disrupts thermogenesis and energy expenditure and increases
90 susceptibility to developing obesity when mice are fed a high fat diet (Hasan et al., 2021). Characterizing
91 the circadian regulation of target pathways offers insight into the pathogenesis and treatment of metabolic
92 syndrome.
93
94 Here, we isolate adipocyte circadian biology from organismal context by comparing circadian
95 transcriptomes of *in vitro* differentiated adipocytes (IVDAs) with *in vivo* brown and white adipose depots.
96 This study used developmentally equivalent cells but excludes input from other cell types and from
97 systemic influences such as feeding, hormones, or body temperature. Accordingly, our experimental
98 design is optimized to capture cell-intrinsic circadian programs in differentiated adipocytes. Our
99 differentiation protocol pushes cells into a committed adipocyte state and does not attempt to capture the
100 adipocyte subtype heterogeneity revealed by single-cell profiling *in vivo* (Maniyadath et al., 2023).
101 Through the systematic comparison of our deeply sequenced transcriptome with comparable datasets
102 derived from whole animals (Zhang et al., 2014), we find that the cell-intrinsic circadian clock regulates
103 the gene expression of fuel oxidation, adipose remodeling, and intra-organ communication programs. We
104 have focused on identifying which pathways rely on systemic signals for their timing as well as the ways

105 in which adipocytes execute these elegant, interlocking pathways. Our findings support the robust
106 circadian timing of mitochondrial oxidative metabolism, energy metabolism, extracellular matrix (ECM)
107 homeostasis, molecular transport, and transcriptional regulation, while phase alignment is selectively
108 shifted by tissue-specific systemic cues. Together, these data demonstrate that adipocyte circadian output
109 is controlled by cell-intrinsic temporal regulatory mechanisms, while tissue-specific systemic cues
110 modulate phase alignment rather than generate rhythmicity *de novo*.
111

112 **RESULTS**

113 **The transcriptome of differentiated adipocytes in culture shows widespread circadian regulation.**
114 We isolated pre-adipocytes of inguinal white adipose tissue (iWAT) obtained from Per2::Luc C57BL/6J
115 mice. The pre-adipocytes were then differentiated *in vitro*, and their clocks synchronized via serum shock
116 and forskolin treatment (see Methods and Supplemental Methods for further details). Synchronized
117 Per2::Luc adipocytes exhibited robust ~24h PER2 oscillations, which were confirmed at the mRNA level
118 by qRT-PCR (Fig. 1A, Fig. S1A-D). Sampling for two replicate time series began at 12 hours post-
119 synchronization (HPS) and continued until 72 HPS. RNA-seq analysis yielded >60M paired-end reads per
120 sample, a depth we chose to detect low-abundance transcripts. To our knowledge, this dataset represents
121 the longest, most deeply sequenced, highest resolution circadian transcriptome for differentiated
122 adipocytes in cell culture to date and has allowed us to detect previously undetected rhythms in CCGs.
123 We performed analysis at the transcript rather than the gene level for protein-coding genes (Fig. S2,
124 Methods, Supplemental Methods). In this dataset, core clock genes were highly circadian, and replicates
125 were almost uniformly in phase (Fig. 1B and Fig. S3). Using ECHO (De Los Santos et al., 2020) and
126 MetaCycle (Wu et al., 2016) with a Benjamini-Hochberg (BH) adjusted p-value ≤ 0.005 and 22-30h
127 period, we identified 4,920 unique circadian transcripts in IVDAs corresponding to 4,346 unique CCGs
128 (21% of the coding transcriptome) (Fig. 1C, D, Supplemental File 1). This represents approximately three
129 times as many CCGs as previously reported for BAT and five as many as was reported for eWAT (cf.
130 Zhang et al., 2014), reflecting use of RNA-seq vs. microarrays, transcript vs. gene level analysis, and

131 ECHO and MetaCycle vs. JTK cycle. ECHO period estimates for rhythmic transcripts in IVDAs are fairly
132 uniform across the detected range (Fig. S4A), the majority of circadian transcripts had BH adj p-values ≤
133 0.005, indicating accurate statistical modeling of these genes by ECHO (Fig. S4B), and the distribution of
134 oscillation types shows approximately equal proportions of harmonic and damped oscillations (Fig. S4C)
135 (De Los Santos et al., 2020). As an independent check of our analysis pipeline, as well as to estimate how
136 many CCGs were primary targets of the core clock, we interrogated our list of CCGs against the 6,276
137 unique BMAL1 target genes identified by iWAT BMAL1 ChIP-seq (Hepler et al., 2022; GEO accession #
138 GSE181443) defining BMAL1-associated targets using a −10 kb to +1 kb window relative to the
139 transcription start site (TSS). The percentage of these CCGs identified as BMAL1 targets does not change
140 significantly as we increase stringency, providing additional validation that our list of CCGs are indeed
141 clock-controlled (Table S1).
142
143 **Comparison of the *in vitro* circadian transcriptome with *in vivo* data from BAT and eWAT.**
144 A principal goal of this study is to ascertain the relative importance of cell-autonomous versus systemic
145 cues in the rhythmicity of adipocytes. To understand how CCGs identified in our study compare to
146 circadian transcriptomes of mouse adipose tissue influenced by systemic cues, we obtained *in vivo* BAT
147 and eWAT (epididymal white adipose tissue) circadian transcriptome data generated using microarrays
148 (Zhang et al., 2014, GEO accession # GSE54652). We filtered genes to remove transcriptional noise as
149 was done for IVDAs, resulting in a detected protein-coding transcriptome of 11,249 genes for BAT and
150 11,624 for eWAT (see Methods, Supplemental Files 2 and 3). To ensure accurate comparisons with our
151 dataset, we reanalyzed these datasets using our analysis. ECHO and MetaCycle identified 4,061 rhythmic
152 protein-coding CCGs in BAT and 3,157 in eWAT. This represents 19.3% for BAT and 15% for eWAT,
153 similar to that calculated for IVDAs (Fig. 1C, D) but higher than previously reported (BAT = 8% and
154 eWAT = 4% of protein-coding genes), reflecting the use of ECHO as well as our application of a wider
155 period range compared to Zhang et al. Circadian time enables us to use a common axis to compare phase
156 between organisms with different free-running period lengths. *Per2* expression is robustly circadian in

every rhythmic mammalian tissue and consistently peaks about 14h after a dark-to-light transition in adipose tissue from mice (Zhang et al., 2014). To assign an estimate of circadian time (CT) to IVDAs, we used the peak of *Per2* expression (22 HPS) following release from synchronization as a phase reference point, assigning this a phase of CT14 and calculating phases for other genes in reference to *Per2*. By this metric, phases of rhythmic core clock component genes or their paralogs in our IVDAs (e.g., *Npas2* and *Clock*) are within 2 hours of those reported from BAT and eWAT *in vivo* (Zhang et al., 2014) (Table S2, Fig. S5). These results demonstrate that the cell-intrinsic TTFL is functioning similarly in IVDAs when compared to adipose tissue, such that observed differences in the phasing of circadian transcripts are not due to differences in the core oscillator, but rather in the circadian physiology of the IVDAs vs. *in vivo*-sampled adipose.

Cell-autonomous circadian regulation of a breadth of processes in adipocytes is frequently further sculpted *in vivo* by cell-extrinsic factors.

To identify which biological pathways were circadianly regulated and determine whether their timing is dependent on systemic cues, we combined standard enrichment analysis with Phase Set Enrichment Analysis (PSEA), both of which utilized Reactome gene sets (Zhang et al., 2016; Milacic et al., 2024) (Fig. 2). We first conducted a Reactome pathway enrichment analysis of all IVDA CCGs using PANTHER (Thomas et al., 2022; Ashburner et al., 2000; The Gene Ontology Consortium, 2023) and identified RHO, CDC42, RAC, and MIRO GTPase pathways, along with membrane trafficking, transcription, RNA and protein metabolism, cell cycle, and signaling pathways, as significantly enriched for circadian genes (FDR ≤ 0.05) (Fig. 2A). Phase-clustered gene sets are defined as gene sets whose expression peaks occur close together in time. Though PANTHER identifies pathways enriched for circadian genes, it does so without regard to peak phase. To determine whether circadian genes in IVDAs, BAT, and eWAT were phase-clustered, we applied Phase Set Enrichment Analysis (PSEA; Zhang et al., 2016). PSEA Kuiper scores quantify the degree to which circadian gene CT values deviate from a uniform distribution, and pathways with Kuiper $q \leq 0.1$ were considered significantly phase-clustered

183 (Methods). Phase clustering strength was further assessed using the vector-average magnitude metric,
184 which reflects temporal cohesiveness within each gene set.
185
186 For easier interpretation and comparison between *in vitro* and *in vivo* datasets we grouped
187 phase-clustered pathways into functional categories using top-level Reactome terms and visualizing the
188 distribution of peak CTs across tissues (Fig. 2B). Although many pathways are shared between IVDAs,
189 BAT, and eWAT, their circadian timing differs systematically by tissue. Most pathways, including those
190 relating to biological process, immune system, protein metabolism and post-translational modifications
191 (PTMs), cell cycle, signal transduction, and transcription generally peak later in IVDAs than *in vivo*
192 depots, indicating widespread temporal repositioning of circadian programs in IVDAs compared to those
193 *in vivo* (Fig. 2). In contrast, the timing of the energy metabolism pathways was more closely aligned
194 between IVDAs and BAT, while eWAT was selectively shifted. ECM homeostasis pathways exhibit
195 conserved timing across all three tissues, clustering near the day-night transition. The timing of molecular
196 transport pathways was coordinated in IVDAs and BAT with no detected phase-clustering in eWAT.
197 Together, these patterns show that circadian pathway timing depends on both functional category and
198 tissue context, with some programs maintaining similar phase relationships.
199
200 To ensure phase clustering isn't driven by the repeated detection of the same circadian genes across
201 related Reactome terms, we performed a PSEA leading-edge overlap analysis. Pairwise Jaccard similarity
202 among the top 50 most overlapping pathways reveals high gene sharing only among cell-cycle-related
203 pathways; most other functional categories show low overlap (Fig. S6). Phase clustering across diverse
204 biological processes arises from independent circadian gene modules rather than a single dominant driver
205 set, consistent with the high overlap between pathways strongly phase clustered and those highly enriched
206 for circadian genes by PANTHER (Fig. S7). Comparison of vector-average magnitude shows no
207 difference among phase-clustered pathways across all tissues (Fig. S8), indicating that systemic cues
208 primarily modulate pathway timing rather than altering overall temporal cohesiveness.

To measure the degree of cell-autonomous versus systemic circadian regulation of phase-clustered pathways, we compared those detected in IVDAs, BAT, and eWAT and found a high overlap (101 pathways in both BAT and IVDAs, 35 in both eWAT and IVDAs, and 33 shared across all three datasets) (Fig. 2C, top and Fig. S10). A higher resolution representation of all phase-clustered pathways further highlights conservation of circadian pathway architecture with depot-specific phase shifts driven by systemic cues (Fig. S11). BAT-IVDA pathways exhibit a consistent average phase delay of about 8-9 hours, whereas no dominant phase-shift pattern was observed for eWAT (Fig. 2C, bottom and Fig. S11). Pathways conserved and in phase across all three depots were dominated by ECM homeostasis, immune signaling, and receptor tyrosine kinase (RTK) pathways (Fig. 2D and Fig. S10). In contrast, 17 pathways were rhythmic in both BAT and eWAT but not in IVDAs, indicating circadian regulation that depends on systemic inputs rather than adipocyte-intrinsic oscillators (Fig. S12). These pathways were enriched for ECM organization, immune and growth factor signaling, and cholesterol biosynthesis, and peaked during late night to early morning (CT20-4) in both depots. Taken together, these results demonstrate that circadian regulation of adipocyte biology is neither purely intrinsic nor purely systemic but rather emerges from the integration of autonomous oscillators with depot-specific physiological cues that sculpt pathway timing *in vivo*.

Clock-organized biological work includes energy metabolism.

Metabolic processes follow a daily rhythm such that anabolic processes (e.g., glycolysis and lipogenesis) primarily occur during the feeding phase and catabolic processes including lipolysis and fatty acid oxidation (FAO) are engaged during fasting (Liu et al., 2025; Lekkas and Paschos, 2019). Reactome metabolic pathways are strongly enriched for CCGs, with pronounced temporal organization in IVDAs (Fig. 3A, B). Lipid-associated pathways are phase-aligned between BAT and IVDAs but diverge in eWAT, indicating depot-specific regulation of adipocyte metabolism (Fig. 3B and Figs. S9-11).

235 The top-level Reactome metabolism pathway shows a significant Kuiper statistic ($6x10^{-4}$) and a very low
236 magnitude (0.14), indicating a bimodal distribution of metabolic CCGs (Fig. 3B, Supplemental File 5).
237 Phase distribution of these genes reveals two dominant peaks: a subjective-day cluster (CT5-16) and a
238 subjective-night cluster (CT17-4) (Fig. 3C). To identify which metabolic processes were specific to each
239 peak, we performed PSEA on the CT5-16 and CT17-4 CCGs independently using only the gene sets
240 which fall under the top-level term of Metabolism. This analysis revealed a clear separation of opposing
241 metabolic processes.
242
243 In mice, which are nocturnal, the subjective day overlaps with the resting period (dawn to dusk) whereas
244 the subjective night overlaps with the active period (dusk to dawn). Pathways phase-clustered exclusively
245 within the CT5-16 window are associated with anabolic and biosynthetic processes, consistent with
246 processes happening during the rest-phase. Pathways phase-clustered exclusively within the CT17-4
247 window are enriched for lipid-centric pathways, including mitochondrial and peroxisomal FAO,
248 phospholipid metabolism, and lipid remodeling which are expected to dominate during the active phase
249 (Hepler et al., 2022) (Fig. 3D). Despite the two windows containing a similar number of CCGs, the
250 nighttime window yielded far more phase-clustered pathways specific to that window suggesting it is the
251 major metabolic window in IVDAs. The CCGs in these pathways were sharply in phase and no genes
252 occur in more than 3 pathways (data not shown), consistent with these being distinct circadianly regulated
253 programs.
254
255 Multiple rate-limiting enzymes within these pathways are circadian in IVDAs and in phase with BAT.
256 Enzymes in glycolysis (*Pfkm, Pfkp*) peak late in the circadian cycle (IVDA CT20, 24; BAT CT20, 2).
257 *Acaca*, which catalyzes the first irreversible step in fatty acid synthesis, is circadian and in phase between
258 IVDA and BAT peaking at CT23 and CT20, respectively. Lipolytic enzymes *Pnpla2 and Lipe* peak at
259 CT2 in IVDAs and CT24 in BAT which coincides with the phase of triglyceride mobilization. Fatty acid
260 oxidation is rhythmically controlled by *Cpt1a, Cpt1b, Acadl, Hadha, Hadhb*, and *Acox1* (Liu et al, 2025)

261 which are tightly phase-clustered in the very early morning (IVDA CT2-4; BAT CT2-6). Oxidative
262 metabolism through the TCA cycle (*Ogdh, Idh2, Mdh1*) and branched-chain amino acid degradation
263 (*Bckdha*) also peaks in this window. Additional rate-limiting steps in phospholipid synthesis (*Gpat3*) and
264 NAD^+ salvage (*Nampt*) peak in phase with lipid handling and mitochondrial function (Supplemental File
265 1 and 2). Together, these data suggest circadian timing preferentially constrains pathways that support
266 sustained oxidative metabolism, with rhythmic pathways sharing similar timing persisting in cultured
267 adipocytes without systemic cues, underscoring their cell-autonomous rhythmicity.
268
269 Pathways associated with the ECM, including integrin and focal adhesion signaling, ECM-receptor
270 interactions, and heparan sulfate and glycosaminoglycan metabolism, show strong phase clustering and
271 peak during the late active to early rest window across IVDAs, BAT, and eWAT (Fig. 2D and Fig. S11).
272 These pathways are in phase with those relating to lipid handling and insulin-related metabolic processes
273 in IVDAs and BAT (Fig. 3D). Adipocyte ECM composition and ECM-cell signaling directly regulate
274 metabolic functions such as insulin-stimulated glucose uptake, adipogenic capacity, and lipid handling,
275 and ECM reprograms adipocyte metabolic phenotypes in a depot-specific manner (Strieder-Barboza et al.,
276 2020; Baker et al., 2017). While circadian regulation of ECM-related pathways has been described in
277 other tissues as a dynamic interface between clocks and cellular function (Dudek et al., 2023), its cell-
278 autonomous circadian regulation has not previously been reported in adipocytes.
279
280 **Molecular transport is cell-autonomously circadianly regulated in IVDAs and BAT.**
281 Molecular transport pathways were enriched for circadian genes in IVDAs (FDR ≤ 0.05). These include
282 vesicle-mediated transport, membrane trafficking, clathrin-mediated endocytosis, and Golgi-to-ER
283 retrograde transport (Fig. 4A). Intra-Golgi and retrograde trafficking pathways show the strongest
284 enrichment and highest circadian gene content (~45%), indicating that intracellular transport pathways are
285 strongly circadianly regulated in IVDAs. Consistent with the enrichment results, PSEA analysis also
286 shows phase-clustering of processes related to molecular transport. Large transport pathways (>100

287 CCGs, Fig. 4B, upper), such as membrane trafficking and vesicle-mediated transport, display more
288 diffuse expression of their CCGs, consistent with continuous transport demand across the circadian day.
289 In contrast, smaller pathways (≤100 CCGs, Fig. 4B, lower) are sharply phase-clustered, peaking primarily
290 during the middle to late subjective day (CT7-14), with plasma lipoprotein assembly and clearance
291 peaking later into the subjective night. Molecular transport pathways are phase-clustered in IVDAs and
292 BAT but not eWAT (Fig. 2B). Although transport pathways peak within a similar circadian window, they
293 are systematically phase-shifted, with BAT peaking near dawn and IVDAs peaking between CT6-11,
294 barring plasma lipoprotein assembly and clearance. Together, these findings indicate that molecular
295 transport follows a cell-intrinsic circadian program whose phase is likely shaped by systemic cues in BAT.
296

297 **Transcriptional and post-transcriptional pathways are strongly phase-clustered and peak late-day**
298 **in IVDAs.**

299 Pathway enrichment analysis also revealed that pathways related to transcriptional regulation, chromatin
300 organization, and RNA metabolic processes are strongly enriched for CCGs in IVDAs (Fig. 5A). These
301 pathways span the multiple stages of gene expression, including chromatin-modification, RNA
302 polymerase II-dependent transcription, and rRNA processing and RNA metabolism, including mRNA
303 splicing. Consistent with these enrichment results, PSEA analysis shows phase-clustering of transcription
304 and post-transcriptional pathways (Fig. 5B). These pathways peak sharply within a narrow circadian
305 window around CT10-12, corresponding to the late light (rest) phase, and nearly antiphase to the timing
306 of the same pathways in BAT (Fig. 2B and Figs. S9-11). This phase offset indicates that systemic cues
307 selectively regulate the timing of transcriptional and post-transcriptional processes *in vivo*.
308

309 **Sequential waves of TF-chromatin engagement in rhythmic BAT chromatin.**

310 To predict how rhythmicity is regulated at the chromatin level, we analyzed rhythmic BAT ATAC-seq
311 peaks (Hepler et al., 2022) grouped into 4-hour Zeitgeber time (ZT) bins. We then performed motif
312 enrichment analysis ($p \leq 1\times10^{-3}$; BH $q \leq 0.01$) on these bins using a curated set of circadian transcription

factor (TF) motifs (39 TFs; 42 position weight matrices) (JASPAR, Ovek Baydar et al., 2025) that are phase-aligned between IVDAs and at least one *in vivo* adipose depot (BAT or eWAT) which allowed us to focus on chromatin patterns that reflect circadian regulation that is likely maintained *in vitro*. This analysis revealed distinct temporal clusters of TF-chromatin engagement across the circadian cycle (Fig. 6A). At the global level, our analysis shows that BAT chromatin accessibility oscillates across circadian time, with two prominent peaks in total ATAC-seq signal at ZT9 and ZT17 despite a largely stable number of accessible regions (Fig. S13). These results suggest that it is rhythmic chromatin accessibility, rather than widespread opening or closing of regulatory elements, that provides a chromatin framework for phase-specific TF engagement.

Motif enrichment in the ZT5-ZT9 bins (early) is dominated by ARNT-family and bHLH-PAS motifs (ARNT, AHR::ARNT, ARNTL), NFIL3/CREB3, and KLF family motifs. The enriched CACGTG E-box motif is annotated as an ARNT-family motif in JASPAR but is also shared by the BMAL1::CLOCK complex. Our analysis shows approximately 70% of the early ZT5 target genes are predicted to be bound by BMAL1 (BMAL1 ChIP-seq peaks in iWAT, Hepler et al., 2022). It is reasonable to assume that this early ARNT enrichment likely reflects clock-dependent chromatin engagement rather than AHR-specific binding, consistent with clock-associated promoter priming near dawn (Menet et al., 2014).

Motifs enriched during the mid-day bin (ZT13) are dominated by nuclear receptor and transcriptional co-regulator motifs, including PPARG::RXRA, NR2F2, TFDP1, and SP1. This enrichment occurs temporally just before the late-day, phase clustered lipid-centric metabolic program identified within the CT17-4 window (Fig. 3D). Motifs enriched during the late-day bins (ZT17-ZT21) are dominated by motifs associated with stress adaptation and feedback regulation, including NFKB2, CLOCK, MAFG::NFE2L1, and CEBPA. This enrichment coincides with the late-day metabolic program identified within the CT17-4 peak. This enrichment profile differs from that reported by Hepler et al. because our

338 analysis was restricted to those TFs that are circadian and in phase between IVDAs and at least one *in*
339 *vivo* adipose dataset.
340
341 Consistent with this temporal organization, enrichment of motifs associated with transcription factors
342 involved in metabolic regulation aligns with the peak expression of several rate-limiting enzymes and key
343 metabolic control points within pathways phase-clustered in the CT17–4 metabolic peak (Fig. 3D). These
344 include enzymes regulating lipid handling, mitochondrial metabolism, energy metabolism, and redox
345 balance: *Lipe, Hadhb*, and *Acox1* (ZT5); *Idh2* and *Nampt* (ZT13); *Pfkp* (ZT17); and *Acadl* (ZT21). These
346 enzymes function within discrete metabolic pathways rather than acting redundantly across multiple
347 pathways, indicating focused circadian regulation at discrete metabolic bottlenecks and coordinated
348 regulation across entire metabolic networks.
349
350 To connect transcription factor (TF)-chromatin engagement with biological function, we performed
351 Reactome pathway enrichment analysis of genes associated with rhythmic BAT chromatin accessibility
352 across the two predominant accessibility peaks (ZT5/9 and ZT13-21) (Fig. S14). Early peaks are
353 dominated by pathways related to transcriptional regulation, RNA metabolism, and signaling. In contrast,
354 the late peaks are dominated by pathways relating to lipid metabolism, phospholipid biosynthesis,
355 mitochondrial function, ECM organization, and nuclear receptor signaling (Fig. 6B).
356
357 Spatial analysis of the Distance-to-TSS of enriched motifs across the circadian day revealed promoter-
358 proximal motifs dominate early (ZT5-ZT9), whereas distal enhancer-associated motifs and higher motif-
359 to-gene ratios increase later (ZT13-ZT17), before finally declining at the end of the circadian day (ZT21)
360 (Fig. S15). These results begin to construct a model where a cell-autonomous relay of TF-chromatin
361 interactions coordinates the temporal progression from early transcriptional and regulatory programs to
362 later metabolic and structural pathway engagement across the circadian cycle.
363

364 **DISCUSSION**

365 To fully understand the role(s) of adipose tissue in mammalian circadian physiology, it is
366 necessary to pursue questions in whole animals, where the full breadth of these systemic actions
367 and interactions can be seen (e.g. Hepler and Bass, 2023; Ribas-Latre et al., 2021; Zhang et al.,
368 2014; Pendergrast et al., 2023). Such studies by design integrate systemic cues such as light/dark,
369 feeding patterns, hormonal regulation, and nutritional status, which influence tissue-specific
370 molecular clocks. However, studying adipose physiology in the context of a whole animal makes
371 it hard to distinguish cell-autonomous regulation from systemic cues, including feedback from
372 one to the other, and thereby potentially difficult to interpret the origins of systemic metabolic
373 mis-regulation. To begin to address this, we generated, to our knowledge, the longest, deepest
374 adipocyte circadian time-course reported to date. This, in combination with ECHO and MetaCycle,
375 allowed us to identify more transcripts and clock-regulated transcripts than previously possible in
376 adipocytes, as well as more rhythmic genes in BAT and eWAT. Using these rhythmic genes, PSEA
377 analyses allowed insights into the nature of cell-autonomous circadian regulation of adipocyte
378 transcriptional output. Beyond this, while it is plain to see that cell-autonomous rhythmicity in IVDAs
379 and *in vivo* is quite pervasive, an attempt to dissect all of this output for all processes risked saying very
380 little about very much. To avoid this and to gain insight into regulatory processes with the goal of
381 revealing cell-autonomous vs. systemic regulation, we concentrated on pathways governing
382 transcriptional regulation, RNA metabolism, molecular transport, ECM, and energy metabolism.
383

384 We identified far more temporally regulated processes in BAT vs IVDAs or eWAT. This increase may
385 suggest that the clock is involved in the regulation of more processes in metabolically active tissues so as
386 to offer a higher degree of metabolic flexibility. There is also a daily rhythm in feeding and body
387 temperature to drive metabolic processes *in vivo*. An organism may benefit from increased circadian
388 regulation in metabolically active tissues to offer a higher degree of metabolic flexibility due in part to
389 fluctuations in the availability of nutrients.

390

391 Agreeing with this observation, many phase-clustered pathways detected by PSEA were shared between
392 IVDAs and BAT, whereas overlap with eWAT was less abundant, which suggests depot-specific
393 differences in the timing of their regulation (Fig. 2C). The circadian clock empowers varying degrees of
394 metabolic flexibility across tissues (Thurley et al., 2017). This is the other side of the same molecular
395 coin; a highly circadianly regulated tissue, like BAT compared to eWAT may be more susceptible to
396 circadian disruption, given that misalignment by systemic cues is proportional to its metabolic flexibility.
397

398 Together, the BAT chromatin accessibility data support the transcriptional similarities observed between
399 IVDAs and BAT and provide a regulatory framework for these shared rhythms. Rhythmic BAT
400 chromatin accessibility follows temporally ordered patterns that align with phase-clustered transcriptional
401 and metabolic programs also present in IVDAs. The correspondence between TF-chromatin engagement,
402 pathway enrichment, and the timing of rate-limiting metabolic enzymes suggests that core aspects of
403 oxidative metabolism, lipid handling, and mitochondrial function are governed by cell-autonomous
404 chromatin programs that are preserved in BAT *in vivo*. These findings indicate that IVDAs capture key
405 regulatory features of BAT metabolism, supporting the idea that shared intrinsic circadian mechanisms
406 underlie their similar transcriptional and metabolic organization, while systemic cues primarily modulate
407 timing rather than defining these programs. Differences between our motif enrichment analysis and prior
408 results reported by Hepler et al. reflect the use of different motif enrichment algorithms and our input list
409 of motifs being restricted to those for TFs that are circadian and in phase between IVDAs and at least one
410 in the *in vivo* dataset. Despite these differences, both analyses converge on a temporally ordered
411 chromatin landscape linking TF engagement with metabolic and mitochondrial pathways in BAT.
412

413 **MATERIALS AND METHODS**

414 **Animals and cell culture.** The inguinal stromal vascular fraction (SVF) was isolated from 8- to 12-week-
415 old homozygous Per2::Luc C57BL/6J mice (N=4) housed at 21±2°C under a 12:12h light/dark cycle and

416 free access to normal chow (PicoLab Verified - 75 IF; 23.3% PRO, 12.9% FAT, 63.7% CHO). Isolated
417 preadipocytes were cultured in "differentiation media" before transfer to "maintenance media". Cells were
418 synchronized for 2-2.5 hours with 50% "base media", 50% FBS (Gibco, lot# 2102306), and 10μM
419 forskolin, then switched to "maintenance media" without dexamethasone and containing 0.01% d-
420 luciferin (100 nM, GoldBio #LUCK-100). Rhythms in luciferase activity were monitored with a
421 Lumicycle to confirm clocks were synchronous across samples. Quantitative PCR of *Per2* was used to
422 confirm synchronicity. See Supplemental Methods and Fig. S1 for further details. Sampling for two
423 replicate time series began at 12 hours post-synchronization (HPS) to avoid artifacts immediately
424 following serum shock (Balsalobre et al., 1998) and continued every 2h with the final sample collected at
425 72 HPS.
426 **RNA extraction, RNA-sequencing and quantification.** Total RNA was extracted from cells using the
427 Qiagen RNeasy Lipid Tissue Mini Kit (Cat #74804, Qiagen) according to manufacturer's protocol.
428 Directional RNA-seq libraries were prepared with ≥ 2μg RNA using rRNA depletion and sequenced to a
429 depth of at least 60M PE reads/sample to allow transcript isoform-level analyses, following the guidelines
430 for detecting low-abundance and isoform-specific circadian transcripts (Li et al., 2015). Reads mapping to
431 any residual ribosomal rRNA were removed using SortMeRNA (Kopylova et al., 2012) and remaining
432 reads were mapped to the *Mus musculus* GRCm38 reference genome and quantified using RSEM version
433 1.3.1 to produce expression in transcripts per million (TPM). See Supplemental Methods for further
434 details.
435 **Filtering of transcripts.** To reduce noise and exclude unexpressed and non-productive transcripts from
436 our analysis, we filtered transcripts to an average Count Per Million (CPM avg) ≥ 10 across all values
437 from replicates and limited our analysis to transcripts that map to protein-coding genes (Fig. S2).
438 Noncoding transcripts were not analyzed and will be the focus of a future manuscript. This filtering
439 process yielded 29,020 transcripts mapping to 13,601 unique genes. For accurate comparison, we
440 similarly filtered BAT and epididymal WAT (eWAT) microarray data from Zhang et al., 2014 to remove
441 transcriptional noise and included only expressed genes. This resulted in a detected protein-coding

442 transcriptome of 11,249 genes for BAT and 11,624 for eWAT. For both IVDAs and *in vivo* datasets, genes
443 under these cutoffs were considered unexpressed and excluded from analysis.
444 **Preprocessing and rhythmicity calling**. The data for IVDAs were preprocessed with LIMBR (Crowell
445 et al., 2019) to remove batch effects. After filtering out noise and unexpressed transcripts (see Fig. S2 and
446 Supplemental Methods), screening for rhythmicity was performed using Extended Circadian Harmonic
447 Oscillator (ECHO; De los Santos et al., 2020). Candidate circadian genes were classified as rhythmic
448 using ECHO based on the following criteria: one or more of their transcripts oscillating with a period of
449 22-30h; oscillation type of harmonic, damped or forced; Benjamini-Hochberg -adjusted p-value ≤ 0.005.
450 This stringent cutoff ensures only the most strongly circadian transcripts were included in our analysis. If
451 more than one transcript passed the requirements for CCG calling the transcript with the lowest BH-adj p-
452 value was selected as the gene's representative transcript. We also used MetaCycle's "meta2d" (Wu et al.,
453 2016) as a complementary algorithm for rhythmicity detection, using the same rhythmicity cutoffs as
454 described above.
455 **Use of PANTHER and PSEA.** Methods and parameters applied for use of PANTHER (gene set
456 enrichment analysis) to identify pathways positively enriched for circadian genes and PSEA (to
457 detect phase-clustered pathways) are fully described in Methods and Supplemental File 4 and 5.
458 **Acknowledgements**
459 We would like to thank Shannon Soucy, Tim Sullivan and Owen Wilkins at the Dartmouth
460 Analytics Core for their consultation on data analysis and interpretation. We would also like to
461 thank Joseph Takahashi who gifted the Per2::Luc mouse prior to the SNP-assisted Speed
462 Congenic crossing at Dartmouth. We would also like to thank Bruce Spiegelman at Harvard
463 Medical School for his valuable advice and guidance in this project.
464 **Funding sources**
465 This work was supported by grants from the National Institutes of Health to J.C.D.
466 (R35GM118021), J.J.L. (R35GM118022) and A. M. F (F31DK131890), COBRE (P20-
467 GM113132), COBRE (P20GM130454).

468 **Author Contributions**

469 Conceived and designed the experiments: JMW, AMF, JJL, JCD. Performed the experiments: JMW and
470 AMF. Analyzed the data: JMW, AMF, PAD. Wrote the paper: JMW, AMF, PAD and JCD.

471 **Data availability**

472 All raw RNA-sequencing data generated in this study have been submitted to the NCBI Gene Expression
473 Omnibus (GEO) repository under accession number GSE202686. eWAT (epididymal white adipose
474 tissue) and BAT (brown adipose tissue) circadian transcriptome data generated by Zhang et al., 2014
475 using microarrays can be found under GEO accession GSE54652**.** BMAL1 ChIP-seq data
476 generated by Hepler et al., 2022 can be found in the GEO repository (GSE181443).

477 **Supplemental Files**

478 Supplemental_Methods.pdf
479 Supplemental_Figures.pdf
480 Supplemental_File_S1.xlsx
481 Supplemental_File_S2.xlsx
482 Supplemental_File_S3.xlsx
483 Supplemental_File_S4.xlsx
484 Supplemental_File_S5.xlsx
485 Supplemental_Table_S1.docx
486 Supplemental_Table_S2.docx
487
488
489
490
491
492
493

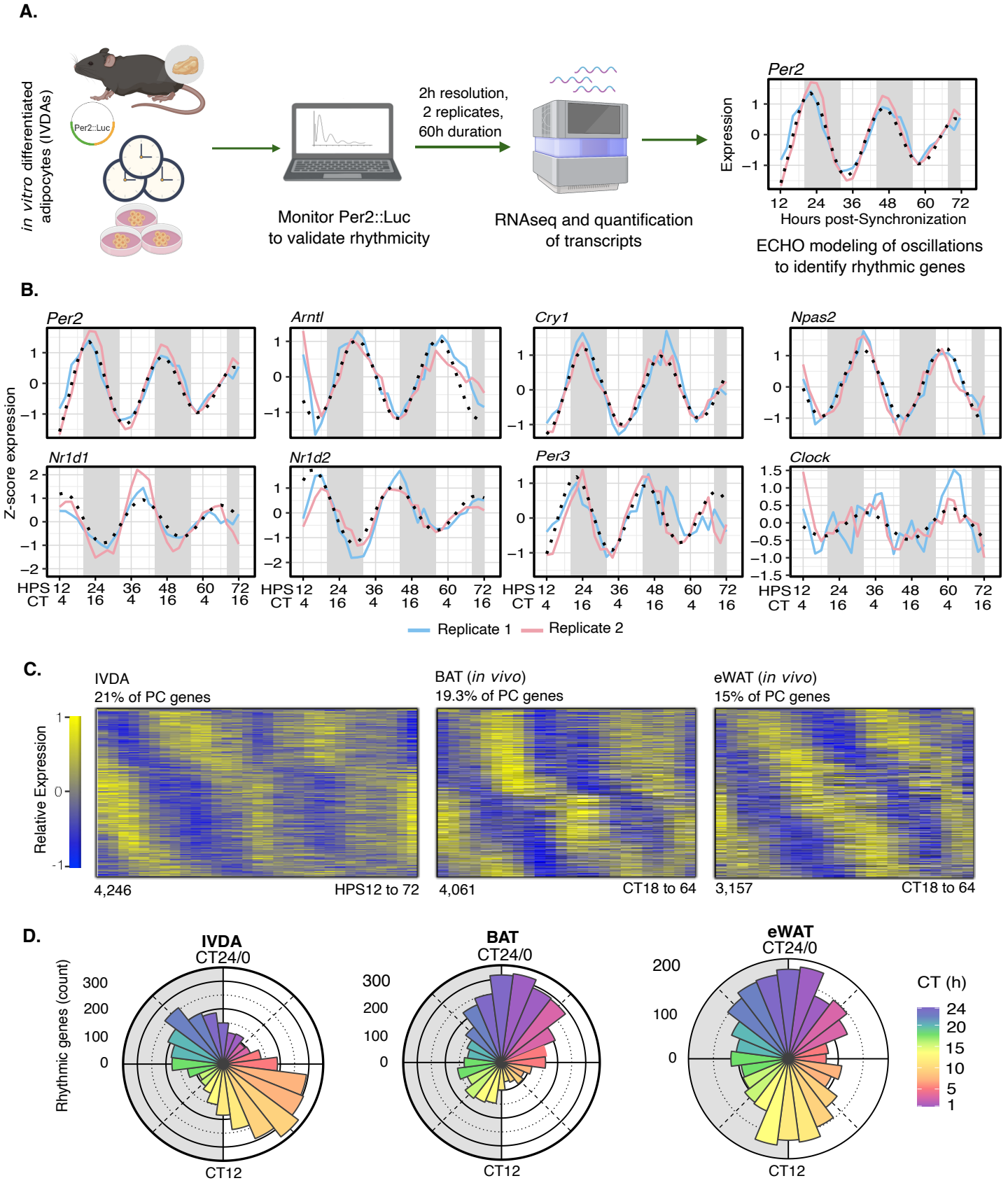

Figure 1. Comparison of the *in vitro* circadian transcriptome with *in vivo* data from BAT and eWAT shows widespread cell-intrinsic circadian regulation.

Figure 1. Comparison of the *in vitro* circadian transcriptome with *in vivo* data from BAT and eWAT shows widespread cell-intrinsic circadian regulation. (A) Diagram of the analysis of adipocyte circadian regulation. Primary inguinal iWAT adipocytes were harvested from Per2::Luc mice and then differentiated and synchronized *in vitro* via serum shock. Two independent time courses were generated. Replicate one and two were sampled every 2 h over 60 h starting at 12 h post-serum shock. ECHO was used to model oscillations and identify circadianly regulated transcripts. Diagram created in BioRender. Worthen, J. (2026) https://BioRender.com/vf15fbu **(B)** Heatmaps showing the relative expressions of circadian transcripts which oscillated with a period of 22-30h and a BH adj P-value of <0.005 in IVDAs, BAT and eWAT. **(C)** Phase distribution of circadian transcripts in IVDAs and brown adipose tissue (BAT) and epididymal white adipose tissue (eWAT) (*in vivo* microarray data, Zhang et al., 2014) shown in circadian time (CT). **(D)** Oscillation of clock genes in Rep1 (pink) and Rep2 (blue) in IVDAs with the ECHO fitted curve shown in black. X-axis is measured in Z-score and y-axis is shown as hours post-synchronization. IVDA = *In Vitro* Differentiated Adipocytes. PC = Protein-Coding.

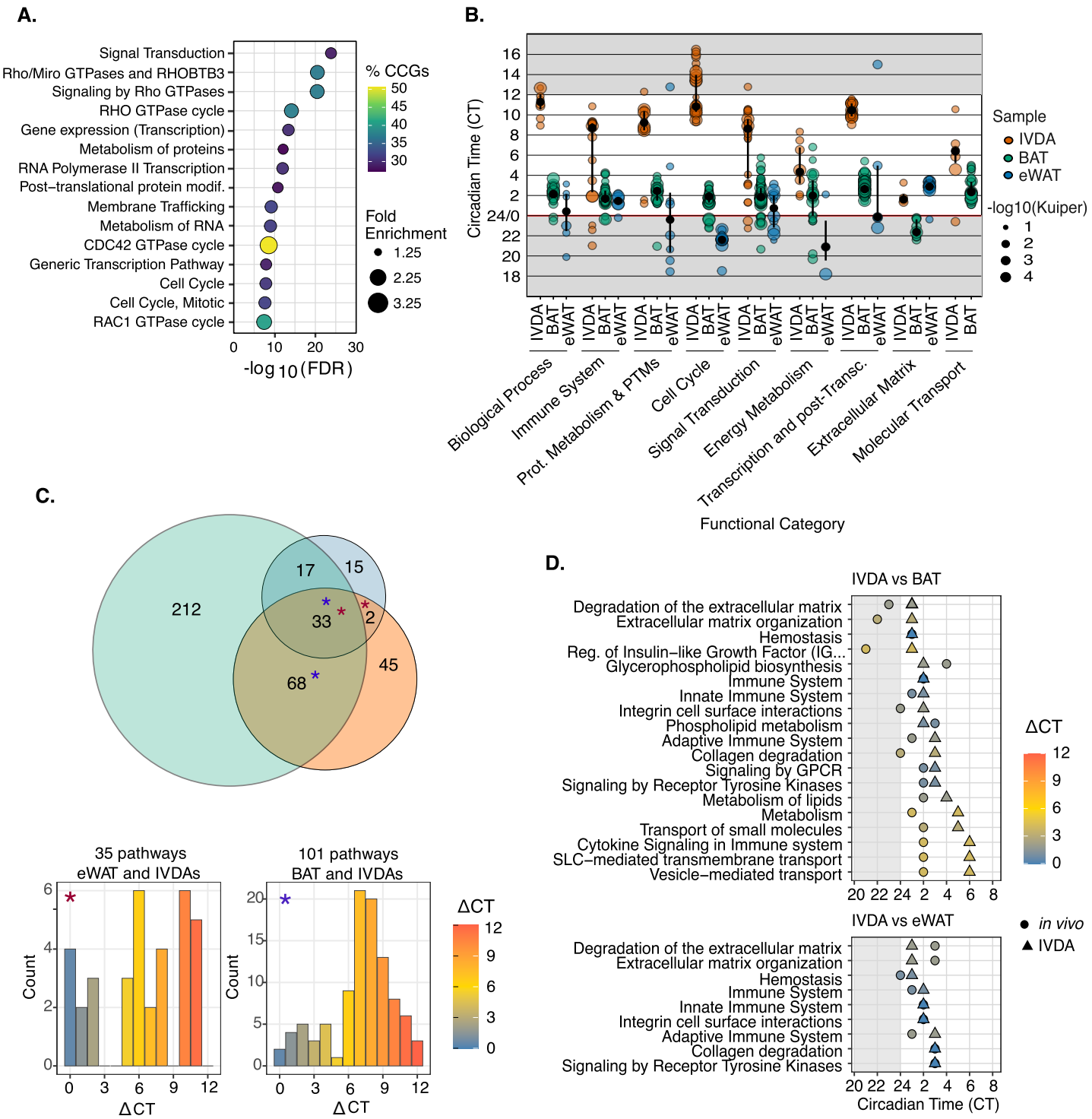

Figure 2. Functional analysis reveals processes that are cell-autonomously circadian yet temporally coordinated by systemic cues. (A) Top 15 Reactome top-level groups most significantly enriched for circadian genes by PANTHER (FDR < 0.05) and significantly phase-clustered by PSEA in IVDA. **(B)** Circadian time (CT) of phase-clustered pathways grouped by Reactome top-level process (colored by sample). Point size = -$\log_{10}$ (q value). Gray shading delineates the four regulatory groups described in text. **(C)** Overlap of rhythmic pathways among IVDA, BAT, and eWAT identified by PSEA. Numbers indicate shared pathway counts; histograms show distributions of phase differences (ΔCT) between IVDA and each *in vivo* depot. The IVDA-BAT histogram shows an average 8-9 h phase delay, indicating substantial temporal re-phasing *in vivo*. **(D)** Representative cell-autonomous rhythmic pathways for IVDA vs BAT (left) and eWAT (right) illustrating phase alignment (<4h) within key top-level processes. ECM pathways, although not enriched for circadian genes, were highly phase-clustered in PSEA, suggesting rhythmic coordination of a smaller, coherent gene subset.

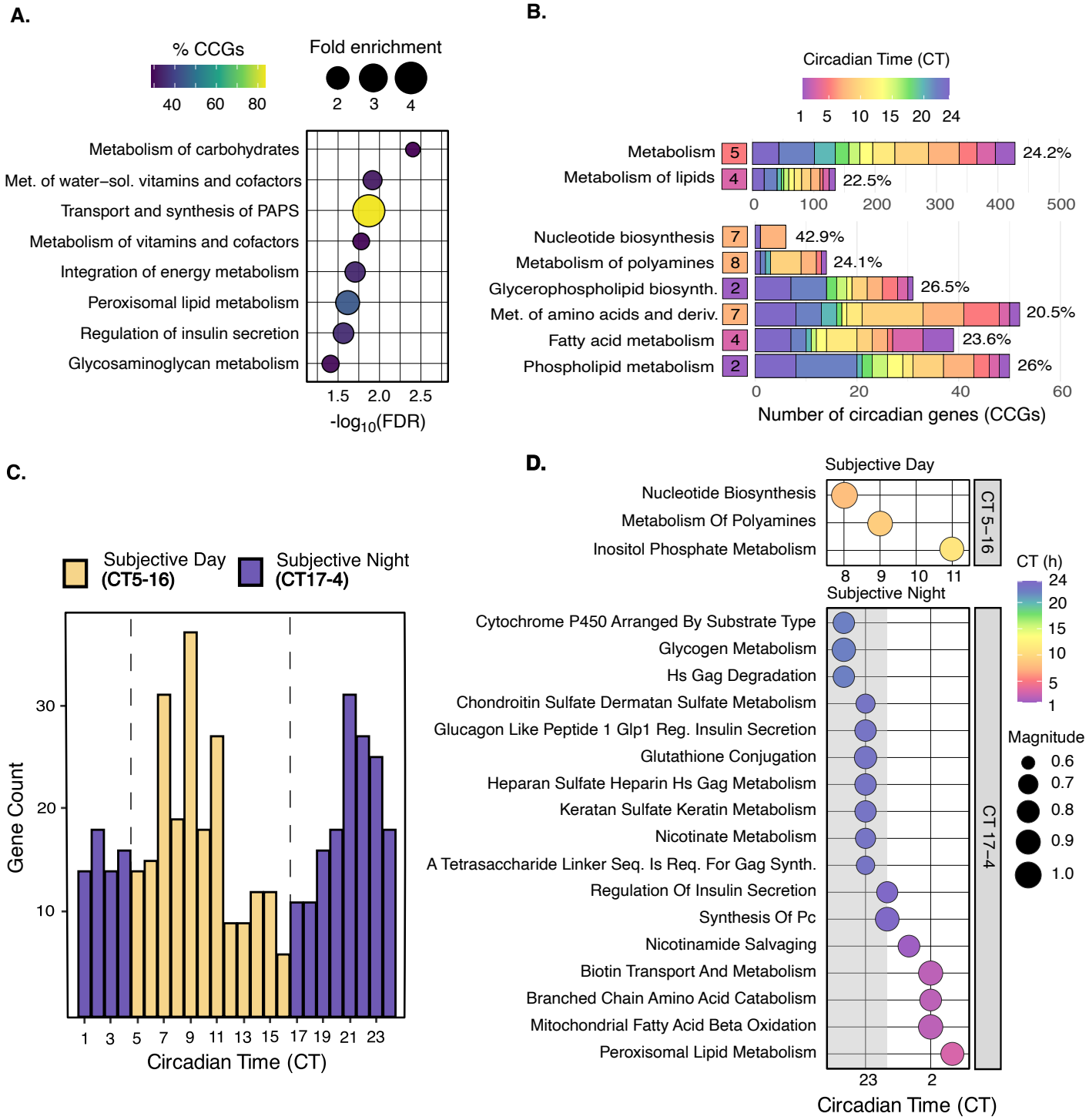

Figure 3. Metabolic sub-pathways display two major circadian waves corresponding to daytime anabolism and nighttime restoration. (A) Reactome energy metabolism pathways ranked by circadian enrichment relative to background. The x-axis indicates -$\log_{10}$(FDR) and dot color represents the percentage of circadian genes in each pathway. Dot size corresponds to fold enrichment. **(B)**. PSEA of Metabolism. Pathways are grouped as Large (> 100 CCGs) or Other (≤ 100 CCGs) and ranked by magnitude. Colored tiles denote mean pathway phase (CT). **(C)** Histogram of all Metabolism circadian transcripts showing two phase peaks (CT 5-16 and CT 17-4). (D) PSEA of Metabolism sub-pathways run separately for Peak 1 and Peak 2 genes. Dot plots show the pathways that were exclusive to either peak 1 (top) or peak 2 (bottom). Color scale = CT; size = magnitude.

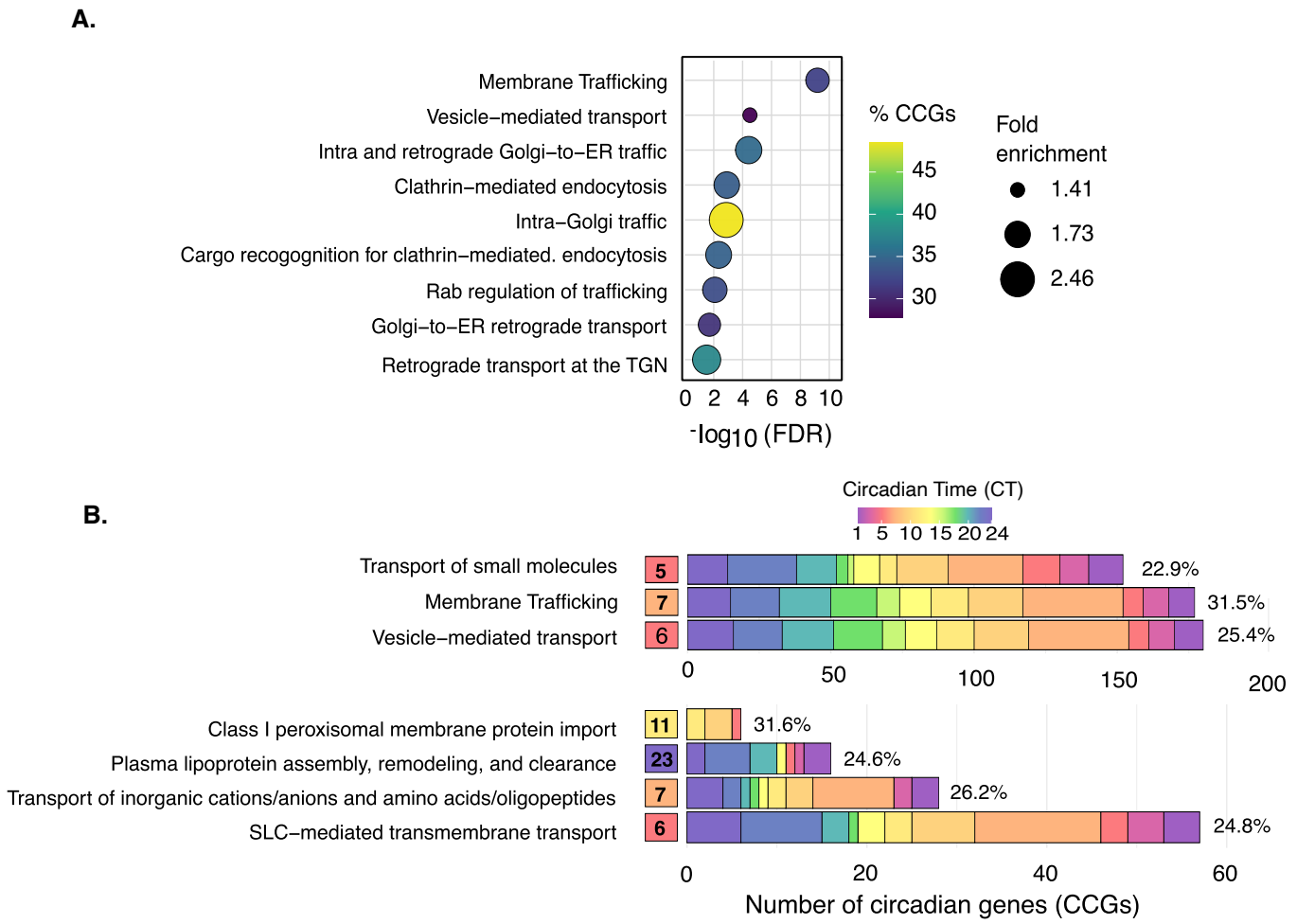

Figure 4. Circadian regulation of molecular transport pathways. (A) Enrichment analysis of Reactome transport-related pathways showing fold enrichment versus FDR significance. The x-axis indicates -$\log_{10}$(FDR) and dot color represents the percentage of circadian genes in each pathway. Dot size corresponds to fold enrichment. Analysis done using Panther.org. **(B)** Circadian phase distribution of circadian genes (CCGs) within large (>100 CCGs) and smaller (≤100 CCGs) molecular transport pathways that were determined to be phase clustered (Kuiper q value < 0.1). Bars show the phase distribution of circadian genes color-coded by 2-hour CT bins. Numbers inside tiles indicate the PSEA calculated peak phase for each pathway. Percentages to the right indicate the fraction of total genes in that Reactome pathway that are rhythmic. Large pathways display broad phase coverage, whereas smaller pathways show sharper, phase-specific clustering.

Figure 5. Transcriptional and RNA metabolic pathways are sharply phase-clustered at CT10-12, indicating a coordinated mid-day transcriptional wave in adipocytes. (A) Dot plot showing enriched transcriptional and RNA-related pathways. The list of pathways was pruned to reduce redundancy. The x-axis indicates -$\log_{10}$(FDR) and dot color represents the percentage of circadian genes in each pathway. Dot size corresponds to fold enrichment. **(B)** Bar plots showing the number and circadian phase (CT) distribution of circadian genes (CCGs) within each pathway. Pathways are divided into large pathways (>100 CCGs; upper panel) and smaller pathways (≤100 CCGs; lower panel). Bars are colored by CT, and numbers on the right indicate the percentage of total circadian genes represented by each pathway. Pathways are ordered by magnitude.

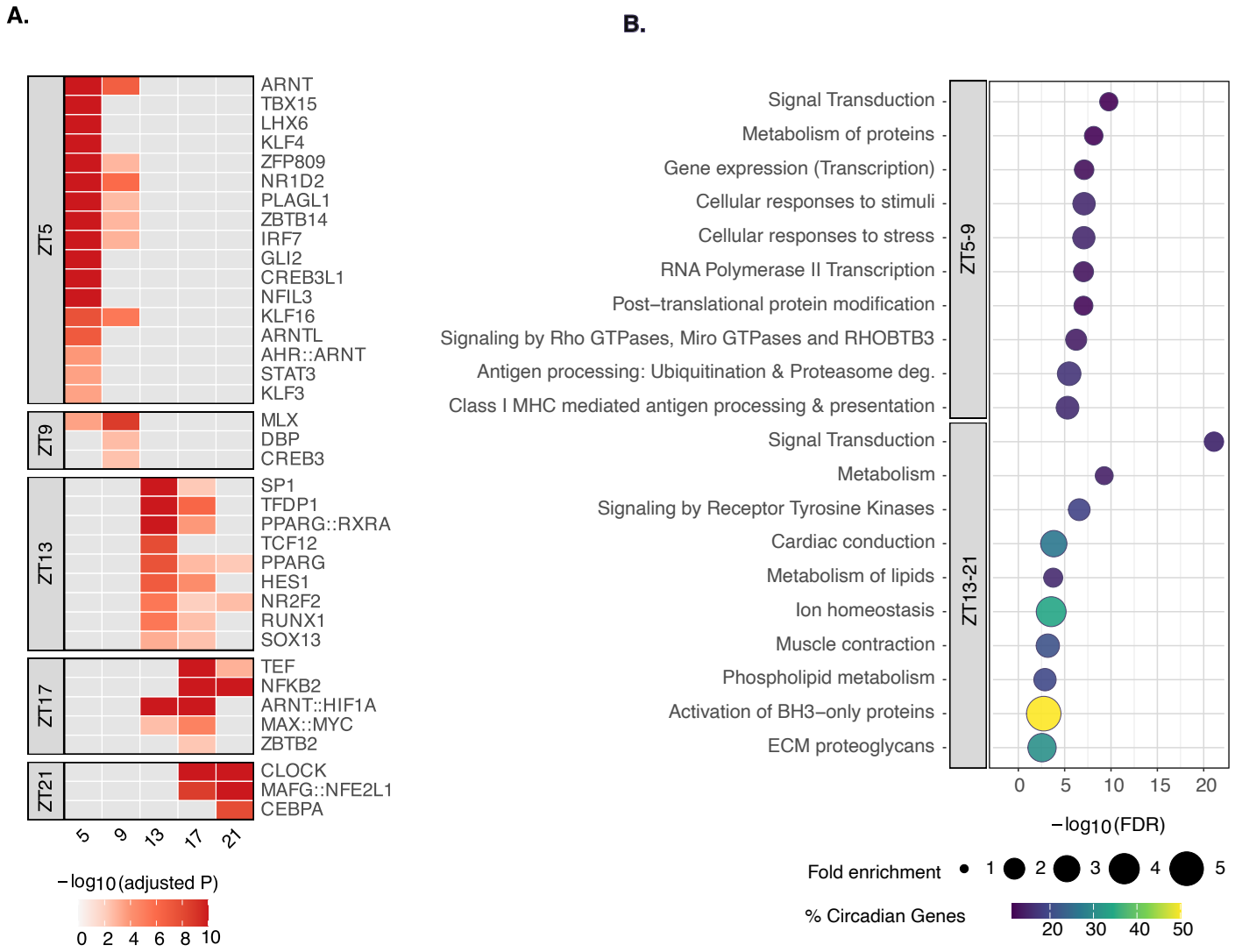

Figure 6. Sequential clusters of circadian transcription factor engagement and pathway enrichment in rhythmic BAT chromatin. (A) Heatmap showing significantly enriched circadian transcription factor (TF) motifs (BH-adjusted $q < 0.01$) across 4-hour Zeitgeber time (ZT) bins in BAT ATAC-seq data. Color indicates -$\log_{10}$(adjusted P-value). Motifs are grouped by the ZT bin at which enrichment is maximal, revealing discrete temporal clusters of TF engagement. **(B)** Reactome pathway enrichment analysis of genes associated with rhythmic BAT chromatin accessibility, summarized across two major temporal clusters (ZT5/9, top and ZT13/17/21, bottom). Dot plots display the top 10 enriched pathways per peak ranked by -$\log_{10}$(FDR). Dot size corresponds to fold enrichment, and color denotes % circadian genes in the pathway.

494 **CITATIONS**

495 Acosta-Rodríguez V, Rijo-Ferreira F, Izumo M, Xu P, Wight-Carter M, Green CB, Takahashi JS. 2022.
496 Circadian alignment of early onset caloric restriction promotes longevity in male C57BL/6J mice. *Science*
497 Jun 10;376(6598):1192-1202. doi: 10.1126/science.abk0297. Epub 2022 May 5. PMID: 35511946;
498 PMCID: PMC9262309.
499

500 Acosta-Rodríguez V, Rijo-Ferreira F, van Rosmalen L, Izumo M, Park N, Joseph C, Hepler C, Thorne
501 AK, Stubblefield J, Bass J, Green CB, Takahashi JS. 2024. Misaligned feeding uncouples daily rhythms
502 within brown adipose tissue and between peripheral clocks. *Cell Rep*. Aug 27;43(8):114523. doi:
503 10.1016/j.celrep.2024.114523. Epub 2024 Jul 23. PMID: 39046875; PMCID: PMC12223410.
504

505 Allada R, Bass J. Circadian Mechanisms in Medicine. 2021. *N Engl J Med* Feb 11;384(6):550-561. doi:
506 10.1056/NEJMra1802337. PMID: 33567194; PMCID: PMC8108270.
507

508 Ashburner M, Ball CA, Blake JA, Botstein D, Butler H, Cherry JM, Davis AP, Dolinski K, Dwight SS,
509 Eppig JT, et al. 2000. Gene ontology: tool for the unification of biology. The Gene Ontology Consortium.
510 *Nat Genet* May;25(1):25-9. doi: 10.1038/75556. PMID: 10802651; PMCID: PMC3037419.
511

512 Baker NA, Muir LA, Washabaugh AR, Neeley CK, Chen SY, Flesher CG, Vorwald J, Finks JF, Ghaferi
513 AA, Mulholland MW, et al. 2017. Diabetes-Specific Regulation of Adipocyte Metabolism by the Adipose
514 Tissue Extracellular Matrix. J Clin *Endocrinol Metab* Mar 1;102(3):1032-1043. doi: 10.1210/jc.2016-
515 2915. PMID: 28359093; PMCID: PMC5460687.
516

517 Balsalobre A, Damiola F, Schibler U. 1998. A serum shock induces circadian gene expression in
518 mammalian tissue culture cells. *Cell* Jun 12;93(6):929-37. doi: 10.1016/s0092-8674(00)81199-x. PMID:
519 9635423.

520

521 Bass J. 2012. Circadian topology of metabolism. *Nature* Nov 15;491(7424):348-56.
522 doi:10.1038/nature11704. PMID: 23151577.
523

524 Bertholet AM, Kazak L, Chouchani ET, Bogaczyńska MG, Paranjpe I, Wainwright GL, Bétourné A,
525 Kajimura S, Spiegelman BM, Kirichok Y. 2017. Mitochondrial Patch Clamp of Beige Adipocytes
526 Reveals UCP1-Positive and UCP1-Negative Cells Both Exhibiting Futile Creatine Cycling. *Cell Metab*
527 Apr 4;25(4):811-822.e4. doi: 10.1016/j.cmet.2017.03.002. PMID: 28380374; PMCID: PMC5448977.
528

529 Bunk J, Hussain MF, Delgado-Martin M, Samborska B, Ersin M, Shaw A, Rahbani JF, Kazak L. 2025.
530 The Futile Creatine Cycle powers UCP1-independent thermogenesis in classical BAT. *Nat Commun* Apr
531 4;16(1):3221. doi: 10.1038/s41467-025-58294-4. PMID: 40185737; PMCID: PMC11971250.
532

533 Cannon B, Nedergaard J. 2004. Brown adipose tissue: function and physiological significance. *Physiol*
534 *Rev* Jan;84(1):277-359. doi: 10.1152/physrev.00015.2003. PMID: 14715917.
535

536 Cao X, Yang Y, Selby CP, Liu Z, Sancar A. 2021. Molecular mechanism of the repressive phase of the
537 mammalian circadian clock. *Proc Natl Acad Sci U S A* Jan 12;118(2):e2021174118.
538 doi:10.1073/pnas.2021174118. Epub 2020 Dec 21. PMID: 33443219; PMCID: PMC7812753.
539

540 Corvera S, Rajan A, Townsend KL, Shamsi F, Wu J, Svensson KJ, Zeltser LM, Collins S, Reis T, Tseng
541 YH, et al. 2026. Advances in Adipose Tissue Biology. *Endocr Rev* Jan 13;47(1):75-92. doi:
542 10.1210/endrev/bnaf032. PMID: 41071598.
543

544 Crowell AM, Greene CS, Loros JJ, Dunlap JC. 2019. Learning and Imputation for Mass-spec Bias
545 Reduction (LIMBR). *Bioinformatics* May 1;35(9):1518-1526. doi:10.1093/bioinformatics/bty828. PMID:
546 30247517; PMCID: PMC6499252.
547
548 Cypess AM, Cannon B, Nedergaard J, Kazak L, Chang DC, Krakoff J, Tseng YH, Schéele C, Boucher J,
549 Petrovic N, et al. 2025. Emerging debates and resolutions in brown adipose tissue research. *Cell Metab*
550 Jan 7;37(1):12-33. doi: 10.1016/j.cmet.2024.11.002. Epub 2024 Dec 6. PMID: 39644896; PMCID:
551 PMC11710994.
552
553 De Los Santos H, Collins EJ, Mann C, Sagan AW, Jankowski MS, Bennett KP, Hurley JM. 2020. ECHO:
554 an application for detection and analysis of oscillators identifies metabolic regulation on genome-wide
555 circadian output. *Bioinformatics* Feb 1;36(3):773-781. doi:10.1093/bioinformatics/btz617. PMID:
556 31384918; PMCID: PMC7523678.
557
558 Deota S, Pendergast JS, Kolthur-Seetharam U, Esser KA, Gachon F, Asher G, Dibner C, Benitah SA,
559 Escobar C, Muoio DM, et al. 2025. The time is now: accounting for time-of-day effects to improve
560 reproducibility and translation of metabolism research. *Nat Metab* Mar;7(3):454-468. doi:
561 10.1038/s42255-025-01237-6. Epub 2025 Mar 17. PMID: 40097742; PMCID: PMC12584160.
562
563 Dudek M, Swift J, Meng QJ. 2023. The circadian clock and extracellular matrix homeostasis in aging and
564 age-related diseases. *Am J Physiol Cell Physiol* Jul 1;325(1):C52-C59. doi:10.1152/ajpcell.00122.2023.
565 Epub 2023 May 29. PMID: 37246635; PMCID: PMC10281784.
566
567 Fekry B, Eckel-Mahan K. 2022. The circadian clock and cancer: links between circadian disruption and
568 disease Pathology. *J Biochem* May 11;171(5):477-486. doi: 10.1093/jb/mvac017. PMID:35191986.
569

570 Hasan N, Nagata N, Morishige JI, Islam MT, Jing Z, Harada KI, Mieda M, Ono M, Fujiwara H, Daikoku
571 T, et al. 2021. Brown adipocyte-specific knockout of Bmal1 causes mild but significant thermogenesis
572 impairment in mice. *Mol Metab* Jul;49:101202. doi: 10.1016/j.molmet.2021.101202. Epub 2021 Mar 3.
573 PMID: 33676029; PMCID: PMC8042177.
574
575 Hepler C, Bass J. 2023. Circadian mechanisms in adipose tissue bioenergetics and plasticity. *Genes Dev*
576 Jun 1;37(11-12):454-473. doi: 10.1101/gad.350759.123. Epub 2023 Jun 26. PMID:37364987; PMCID:
577 PMC10393195.
578
579 Hepler C, Weidemann BJ, Waldeck NJ, Marcheva B, Cedernaes J, Thorne AK, Kobayashi Y, Nozawa R,
580 Newman MV, Gao P, et al. 2022. Time-restricted feeding mitigates obesity through adipocyte
581 thermogenesis. *Science* Oct 21;378(6617):276-284. doi: 10.1126/science.abl8007. Epub 2022 Oct 20.
582 PMID: 36264811; PMCID: PMC10150371.
583
584 Hurley JM, Loros JJ, Dunlap JC. 2016. The circadian system as an organizer of metabolism. *Fungal*
585 *Genet Biol* May;90:39-43. doi: 10.1016/j.fgb.2015.10.002. Epub 2015 Oct 20. PMID:26498192; PMCID:
586 PMC4818683.
587
588 Inagaki T, Sakai J, Kajimura S. 2016. Transcriptional and epigenetic control of brown and beige adipose
589 cell fate and function. *Nat Rev Mol Cell Biol* Aug;17(8):480-95. doi:10.1038/nrm.2016.62. Epub 2016
590 Jun 2. Erratum in: Nat Rev Mol Cell Biol. 2017Aug;18(8):527. doi: 10.1038/nrm.2017.72. PMID:
591 27251423; PMCID: PMC4956538.
592
593 Kettner NM, Mayo SA, Hua J, Lee C, Moore DD, Fu L. 2015. Circadian Dysfunction Induces Leptin
594 Resistance in Mice. *Cell Metab* Sep 1;22(3):448-59. doi: 10.1016/j.cmet.2015.06.005.Epub 2015 Jul 9.
595 PMID: 26166747; PMCID: PMC4558341.

596

597 Kiehn JT, Tsang AH, Heyde I, Leinweber B, Kolbe I, Leliavski A, Oster H. 2017. Circadian Rhythms in
598 Adipose Tissue Physiology. *Compr Physiol* Mar 16;7(2):383-427. doi:10.1002/cphy.c160017. PMID:
599 28333377.

600

601 Kopylova E, Noé L, Touzet H. 2012. SortMeRNA: fast and accurate filtering of ribosomal RNAs in
602 metatranscriptomic data. *Bioinformatics* Dec 15;28(24):3211–3217. doi:10.1093/bioinformatics/bts611.
603 PMID: 23071270.

604

605 Lekkas D, Paschos GK. 2019. The circadian clock control of adipose tissue physiology and metabolism.
606 *Auton Neurosci* Jul;219:66-70. doi: 10.1016/j.autneu.2019.05.001. Epub 2019 May 8. PMID: 31122604.

607

608 Li J, Grant GR, Hogenesch JB, Hughes ME. 2015. Considerations for RNA-seq analysis of circadian
609 rhythms. *Methods Enzymol* 2015;551:349-67. doi: 10.1016/bs.mie.2014.10.020. Epub 2014 Dec26.
610 PMID: 25662464.

611

612 Liu H, Wang S, Wang J, Guo X, Song Y, Fu K, Gao Z, Liu D, He W, Yang LL. 2025. Energy metabolism
613 in health and diseases. *Signal Transduct Target Ther* Feb 18;10(1):69. doi: 10.1038/s41392-025-02141-x.
614 PMID: 39966374; PMCID: PMC11836267.

615

616 Loft A, Emont MP, Weinstock A, Divoux A, Ghosh A, Wagner A, Hertzel AV, Maniyadath B,
617 Deplancke B, Liu B, et al. 2025. Towards a consensus atlas of human and mouse adipose tissue at single-
618 cell resolution. *Nat Metab* May;7(5):875-894. doi: 10.1038/s42255-025-01296-9. Epub 2025 May 13.
619 PMID: 40360756; PMCID: PMC12707904.

620

621 Malik DM, Rhoades SD, Zhang SL, Sengupta A, Barber A, Haynes P, Arnadottir ES, Pack A, Kibbey
622 RG, Kain P, et al. 2024. Glucose Challenge Uncovers Temporal Fungibility of Metabolic Homeostasis
623 over a day:night cycle. *bioRxiv* [Preprint]. Aug 21:2023.10.30.564837. doi: 10.1101/2023.10.30.564837.
624 PMID: 37961230; PMCID: PMC10634956.
625
626 Maniyadath B, Zhang Q, Gupta RK, Mandrup S. 2023. Adipose tissue at single-cell resolution. *Cell*
627 *Metab* 35(3):386–413. Mar 7. doi: 10.1016/j.cmet.2023.02.002. PMID: 36870444; PMCID:
628 PMC10021468.
629
630 Menet JS, Pescatore S, Rosbash M. 2014. CLOCK:BMAL1 is a pioneer-like transcription factor. *Genes*
631 *Dev* Jan 1;28(1):8-13. doi: 10.1101/gad.228536.113. PMID: 24395244; PMCID:PMC3894415.
632
633 Milacic M, Beavers D, Conley P, Gong C, Gillespie M, Griss J, Haw R, Jassal B, Matthews L, May B, et
634 al. 2024. The Reactome Pathway Knowledgebase 2024. *Nucleic Acids Res* Jan 5;52(D1):D672-D678. doi:
635 10.1093/nar/gkad1025. PMID: 37941124; PMCID: PMC10767911.
636
637 Narasimamurthy R, Virshup DM. 2021. The phosphorylation switch that regulates ticking of the circadian
638 clock. *Mol Cell* Mar 18;81(6):1133-1146. doi: 10.1016/j.molcel.2021.01.006. Epub 2021 Feb 4. PMID:
639 33545069.
640
641 Neufeld-Cohen A, Robles MS, Aviram R, Manella G, Adamovich Y, Ladeuix B, Nir D, Rousso-Noori L,
642 Kuperman Y, Golik M, et al. 2016. Circadian control of oscillations in mitochondrial rate-limiting
643 enzymes and nutrient utilization by PERIOD proteins. *Proc Natl Acad Sci U S A* Mar 22;113(12):E1673-
644 82. doi: 10.1073/pnas.1519650113. Epub 2016 Feb 9. PMID: 26862173; PMCID: PMC4812734.
645

646 Ovek Baydar D, Rauluseviciute I, Aronsen DR, Blanc-Mathieu R, Bonthuis I, de Beukelaer H, Ferenc K,
647 Jegou A, Kumar V, Lemma RB, et al. 2026. JASPAR 2026: expansion of transcription factor binding
648 profiles and integration of deep learning models. *Nucleic Acids Res* Jan 6;54(D1):D184-D193. doi:
649 10.1093/nar/gkaf1209. PMID: 41325984; PMCID: PMC12807658.
650
651 Pendergrast LA, Lundell LS, Ehrlich AM, Ashcroft SP, Schönke M, Basse AL, Krook A, Treebak JT,
652 Dollet L, Zierath JR. 2023. Time of day determines postexercise metabolism in mouse adipose tissue.
653 *Proc Natl Acad Sci U S A* Feb 21;120(8):e2218510120. doi: 10.1073/pnas.2218510120. Epub 2023 Feb
654 13. PMID: 36780527; PMCID: PMC9974500.
655
656 Philpott JM, Freeberg AM, Park J, Lee K, Ricci CG, Hunt SR, Narasimamurthy R, Segal DH, Robles R,
657 Cai Y, Tripathi S, McCammon JA, Virshup DM, Chiu JC, Lee C, Partch CL. 2023. PERIOD
658 phosphorylation leads to feedback inhibition of CK1 activity to control circadian period. *Mol Cell* May
659 18;83(10):1677-1692.e8. doi: 10.1016/j.molcel.2023.04.019. PMID: 37207626; PMCID: PMC11684667.
660
661 Puigserver P, Wu Z, Park CW, Graves R, Wright M, Spiegelman BM. 1998. A cold-inducible coactivator
662 of nuclear receptors linked to adaptive thermogenesis. *Cell* Mar 20;92(6):829-39. doi: 10.1016/s0092-
663 8674(00)81410-5. PMID: 9529258.
664
665 Rahbani JF, Bunk J, Lagarde D, Samborska B, Roesler A, Xiao H, Shaw A, Kaiser Z, Braun JL,
666 Geromella MS, et al. 2024. Parallel control of cold-triggered adipocyte thermogenesis by UCP1 and
667 CKB. *Cell Metab* Mar 5;36(3):526-540.e7. doi: 10.1016/j.cmet.2024.01.001. Epub 2024 Jan 24. PMID:
668 38272036.
669

670 Rasmussen ES, Takahashi JS, Green CB. 2022. Time to target the circadian clock for drug discovery.
671 *Trends Biochem Sci* Sep;47(9):745-758. doi: 10.1016/j.tibs.2022.04.009. Epub 2022 May 13. PMID:
672 35577675; PMCID: PMC9378619.
673
674 Ribas-Latre A, Santos RB, Fekry B, Tamim YM, Shivshankar S, Mohamed AMT, Baumgartner C, Kwok
675 C, Gebhardt C, Rivera A, et al. 2021. Cellular and physiological circadian mechanisms drive diurnal cell
676 proliferation and expansion of white adipose tissue. *Nat Commun* Jun 9;12(1):3482. doi: 10.1038/s41467-
677 021-23770-0.
678
679 Ricci CG, Philpott JM, Torgrimson MR, Freeberg AM, Narasimamurthy R, Pécora de Barros E, Amaro
680 R, Virshup DM, McCammon JA, Partch CL. 2025. Markovian state models uncover casein kinase 1
681 dynamics that govern circadian period. *Biophys J* Nov 18;124(22):4034-4048. doi:
682 10.1016/j.bpj.2025.09.022. Epub 2025 Sep 18. PMID: 40968534; PMCID: PMC12709424.
683
684 Roh HC, Tsai LTY, Shao M, Tenen D, Shen Y, Kumari M, Lyubetskaya A, Jacobs C, Dawes B, Gupta
685 RK, et al. 2018. Warming Induces Significant Reprogramming of Beige, but Not Brown, Adipocyte
686 Cellular Identity. *Cell Metab* May 1;27(5):1121-1137.e5. doi: 10.1016/j.cmet.2018.03.005. Epub 2018
687 Apr 12. PMID: 29657031; PMCID: PMC5932137.
688
689 Rosen ED, Spiegelman BM. 2006. Adipocytes as regulators of energy balance and glucose homeostasis.
690 *Nature* Dec 14;444(7121):847-53. doi: 10.1038/nature05483. PMID:17167472; PMCID: PMC3212857.
691
692 Sakers A, De Siqueira MK, Seale P, Villanueva CJ. 2022. Adipose-tissue plasticity in health and disease.
693 *Cell* Feb 3;185(3):419-446. doi: 10.1016/j.cell.2021.12.016. PMID: 35120662;PMCID: PMC11152570.
694

695 Samanta S, Ali SA. 2022. Impact of circadian clock dysfunction on human health. *Explor neurosci* 1(1),
696 Article 1. https://doi.org/10.37349/en.2022.00002.
697
698 Scheer FA, Hilton MF, Mantzoros CS, Shea SA. 2009. Adverse metabolic and cardiovascular
699 consequences of circadian misalignment. *Proc Natl Acad Sci U S A* Mar 17;106(11):4453-8. doi:
700 10.1073/pnas.0808180106. Epub 2009 Mar 2. PMID: 19255424; PMCID: PMC2657421.
701
702 Schrader LA, Ronnekleiv-Kelly SM, Hogenesch JB, Bradfield CA, Malecki KM. 2024. Circadian
703 disruption, clock genes, and metabolic health. *J Clin Invest* Jul 15;134(14):e170998. doi:
704 10.1172/JCI170998. PMID: 39007272; PMCID: PMC11245155.
705
706 Smyllie NJ, Koch AA, Adamson AD, Patton AP, Johnson A, Bagnall JS, Johnson O, Meng QJ, Loudon
707 ASI, Hastings MH. 2025. Quantitative measures of clock protein dynamics in the mouse suprachiasmatic
708 nucleus extends the circadian time-keeping model. *EMBO J* Jul;44(13):3614-3644. doi: 10.1038/s44318-
709 025-00426-z. Epub 2025 Apr 17. PMID: 40247113; PMCID: PMC12218236.
710
711 Strieder-Barboza C, Baker NA, Flesher CG, Karmakar M, Patel A, Lumeng CN, O'Rourke RW. 2020.
712 Depot-specific adipocyte-extracellular matrix metabolic crosstalk in murine obesity. *Adipocyte*
713 Dec;9(1):189-196. doi: 10.1080/21623945.2020.1749500. PMID: 32272860; PMCID: PMC7153651.
714
715 Sun Y, Rahbani JF, Jedrychowski MP, Riley CL, Vidoni S, Bogoslavski D, Hu B, Dumesic PA, Zeng X,
716 Wang AB, et al. 2021. Mitochondrial TNAP controls thermogenesis by hydrolysis of phosphocreatine.
717 *Nature* May;593(7860):580-585. doi: 10.1038/s41586-021-03533-z. Epub 2021 May 12. PMID:
718 33981039; PMCID: PMC8287965.
719

720 Takahashi JS. Transcriptional architecture of the mammalian circadian clock. 2017. *Nat Rev Genet*
721 Mar;18(3):164-179. doi: 10.1038/nrg.2016.150. Epub 2016 Dec 19. PMID: 27990019; PMCID:
722 PMC5501165.
723
724 The Gene Ontology Consortium; Aleksander SA, Balhoff J, Carbon S, Cherry JM, Drabkin HJ, Ebert D,
725 Feuermann M, Gaudet P, Harris NL, Hill DP, et al. 2023. The Gene Ontology knowledgebase in 2023.
726 *Genetics* May 4;224(1):iyad031. doi: 10.1093/genetics/iyad031. PMID: 36866529; PMCID:
727 PMC10158837.
728
729 Thomas PD, Ebert D, Muruganujan A, Mushayahama T, Albou LP, Mi H. 2022. PANTHER: Making
730 genome-scale phylogenetics accessible to all. *Protein Sci* Jan;31(1):8-22. doi:10.1002/pro.4218. Epub
731 2021 Nov 25. PMID: 34717010; PMCID: PMC8740835.
732
733 Thurley K, Herbst C, Wesener F, Koller B, Wallach T, Maier B, Kramer A, Westermark PO. 2017.
734 Principles for circadian orchestration of metabolic pathways. *Proc Natl Acad Sci U S A* Feb
735 14;114(7):1572-1577. doi: 10.1073/pnas.1613103114. Epub 2017 Feb 3. PMID: 28159888; PMCID:
736 PMC5321018.
737
738 Van Drunen R, Eckel-Mahan K. 2021. Circadian Rhythms of the Hypothalamus: From Function to
739 Physiology. *Clocks Sleep* Feb 25;3(1):189-226. doi: 10.3390/clockssleep3010012. PMID:33668705;
740 PMCID: PMC7931002.
741
742 van Rosmalen L, Deota S, Maier G, Le HD, Lin T, Ramasamy RK, Hut RA, Panda S. 2024. Energy
743 balance drives diurnal and nocturnal brain transcriptome rhythms. *Cell Rep* Mar 26;43(3):113951. doi:
744 10.1016/j.celrep.2024.113951. Epub 2024 Mar 19. PMID: 38508192; PMCID: PMC11330649.
745

Vargas-Castillo A, Sun Y, Smythers AL, Grauvogel L, Dumesic PA, Emont MP, Tsai LT, Rosen ED, Zammit NW, Shaffer SM, et al. 2024. Development of a functional beige fat cell line uncovers independent subclasses of cells expressing UCP1 and the futile creatine cycle. *Cell Metab* Sep 3;36(9):2146-2155.e5. doi: 10.1016/j.cmet.2024.07.002. Epub 2024 Jul 30. PMID: 39084217; PMCID: PMC12005060.

Wu G, Anafi RC, Hughes ME, Kornacker K, Hogenesch JB. 2016. MetaCycle: an integrated R package to evaluate periodicity in large scale data. *Bioinformatics* Nov 1;32(21):3351-3353. doi: 10.1093/bioinformatics/btw405. Epub 2016 Jul 4. PMID: 27378304; PMCID: PMC5079475.

Xiong X, Lin Y, Lee J, Paul A, Yechoor V, Figueiro M, Ma K. 2021. Chronic circadian shift leads to adipose tissue inflammation and fibrosis. *Mol Cell Endocrinol* Feb 5;521:111110. doi:10.1016/j.mce.2020.111110. Epub 2020 Dec 4. PMID: 33285245; PMCID: PMC7799174.

Yang Loureiro Z, Solivan-Rivera J, Corvera S. 2022. Adipocyte Heterogeneity Underlying Adipose Tissue Functions. *Endocrinology* Jan 1;163(1):bqab138. doi: 10.1210/endocr/bqab138. PMID: 34223880; PMCID: PMC8660558.

Ye L, Wu J, Cohen P, Kazak L, Khandekar MJ, Jedrychowski MP, et al. 2013. Fat cells directly sense temperature to activate thermogenesis. P*roc Natl Acad Sci U S A* Jul 23;110(30):12480-12485. doi: 10.1073/pnas.1310261110. PMID: 23818608; PMCID: PMC3725076.

Zhang R, Lahens NF, Ballance HI, Hughes ME, Hogenesch JB. 2014. A circadian gene expression atlas in mammals: implications for biology and medicine. *Proc Natl Acad Sci U S A* Nov 11;111(45):16219-24. doi: 10.1073/pnas.1408886111. Epub 2014 Oct 27. PMID: 25349387; PMCID: PMC4234565.

Zhang R, Podtelezhnikov AA, Hogenesch JB, Anafi RC. 2016. Discovering Biology in Periodic Data through Phase Set Enrichment Analysis (PSEA). *J Biol Rhythms* Jun;31(3):244-57. doi: 10.1177/0748730416631895. Epub 2016 Mar 8. PMID: 26955841.

Zvonic S, Ptitsyn AA, Conrad SA, Scott LK, Floyd ZE, Kilroy G, Wu X, Goh BC, Mynatt RL, Gimble JM. 2006. Characterization of peripheral circadian clocks in adipose tissues. *Diabetes* Apr;55(4):962-70. doi: 10.2337/diabetes.55.04.06.db05-0873. PMID: 16567517.